Identification of Ultrafast Relaxation Processes As a Major Reason for Inefficient Exciton Diffusion in Perylene-Based Organic Semiconductors

Volker Settels,[†] Alexander Schubert,[†,⊥] Maxim Tafipolski,[†] Wenlan Liu,[†,#] Vera Stehr,[‡] Anna K. Topczak,[‡,§] Jens Pflaum,[‡,§] Carsten Deibel,[‡] Reinhold F. Fink,[†,∥] Volker Engel,[†] and Bernd Engels*,[†]

[†]Institut für Physikalische und Theoretische Chemie, Universität Würzburg, Emil-Fischer-Str. 42, 97074 Würzburg, Germany

[‡]Lehrstuhl für Experimentelle Physik VI, Universität Würzburg, Am Hubland, 97074 Würzburg, Germany

[§]ZAE Bayern e.V., Am Galgenberg 87, 97074 Würzburg, Germany

S *Supporting Information*

ABSTRACT: The exciton diffusion length (L_D) is a key parameter for the efficiency of organic optoelectronic devices. Its limitation to the nm length scale causes the need of complex bulk-heterojunction solar cells incorporating difficulties in long-term stability and reproducibility. A comprehensive model providing an atomistic understanding of processes that limit exciton trasport is therefore highly desirable and will be proposed here for perylene-based materials. Our model is based on simulations with a hybrid approach which combines high-level ab initio computations for the part of the system directly involved in the described processes with a force field to include environmental effects. The adequacy of the model is shown by detailed comparison with available experimental results. The model indicates that the short exciton diffusion lengths of α-perylene tetracarboxylicdianhydride (PTCDA) are due to ultrafast relaxation processes of the optical excitation via intermolecular motions leading to a state from which further exciton diffusion is hampered. As the efficiency of this mechanism depends strongly on molecular arrangement and environment, the model explains the strong dependence of L_D on the morphology of the materials, for example, the differences between α-PTCDA and diindenoperylene. Our findings indicate how relaxation processes can be diminished in perylene-based materials. This model can be generalized to other organic compounds.
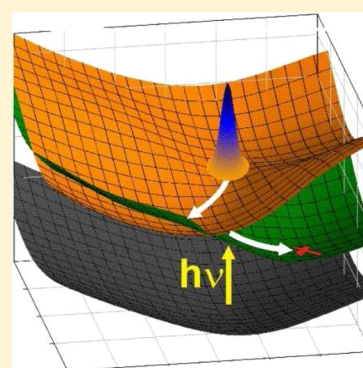
INTRODUCTION

Organic semiconductors are promising materials for thin-film electronic devices such as organic solar cells. Especially for the latter, however, their efficiencies are strongly limited due to small exciton diffusion lengths (L_D).[1,2] Organic solar cells have been tremendously improved in recent years, often by trial-and-error variations of materials and device architecture,[3−6] but further optimization requires a better understanding of the underlying microscopic and atomistic power conversion processes.[7,8] More efficient exciton diffusion is desirable since this improves device efficiencies and allows to use less complex device architectures.[7] In order to design compounds with extended exciton diffusion lengths (L_D), a detailed knowledge about possible loss processes such as exciton trapping is needed.

Trapping processes which shorten L_D were carefully investigated by various experiments, but a comprehensive model providing an atomistic understanding of these processes[8,9] and their influence on L_D[10,11] is still missing. In the case of perylene-based materials, absorption and emission spectra of aggregates, crystals, and thin films pointed toward population transfers from locally excited Frenkel states to spatially separated charge-transfer (CT) states.[11,12] However, these explanations were questioned by recent experiments on neat organic semiconductors, which indicated that the CT states lie energetically above their Frenkel counterparts.[5,6,13,14] Theoretical descriptions supporting the transfer to CT states by simulations based on empirical Hamiltonians[15,16] were furthermore challenged by high-level ab initio calculations which support the recent experiments.[17−19] For perylene tetracarboxylic bisimide (PBI) thin-films transient absorption measurements identified a fast relaxation (∼100 ps) of the exciton to an intermolecular, long-lived (∼20 ns), immobile state which exhibits a red-shifted emission spectrum.[20] Time-dependent spectroscopy on PBI-doped films indicated that dimer states can constitute efficient exciton traps.[21] Raman spectroscopic measurements of α-perylene single crystals indicated that exciton self-trapping is triggered by motions of two monomers relative to each other.[10] A corresponding atomistic model was provided in a recent ab initio-based simulation of PBI aggregates which revealed an efficient self-

trapping due to photoinduced intermolecular motions.[17,22] Corresponding exciton–phonon coupling models have also been discussed in theoretical works on exciton confinement[23,24] or relaxation to CT states.[15,16,25] Recently, it has been shown theoretically that, using two-dimensional electronic spectroscopy, the photoinduced intermolecular torsional motion yielding a crossing of the adiabatic excitonic potential surfaces could be distinguished from a competitive direct exciton relaxation due to coupling to the environment in solution.[26]

Recent experiments also provide evidence that the molecular packing motif in the solid state has a significant influence on exciton self-trapping.[27,28] As an elucidative example, measurements of L_D for single crystalline layers showed large differences between the two perylene derivatives (see Scheme 1) α-perylene tetracarboxylic dianhydride (α-PTCDA; L_D =

Scheme 1. Perylene-Based Molecules Considered in This Work: PTCDA (left) and DIP (right)
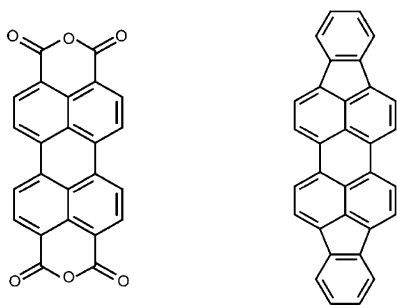
22 nm)[29] and diindenoperylene (DIP; L_D = 100 nm).[30] Recently, some of us proposed a theoretical approach to estimate exciton diffusion lengths based on the hopping model and a Marcus approach that employed quantum chemical results for electronic couplings and relaxation energies. This model predicts a L_D value of 160 nm for α-PTCDA, which is almost an order of magnitude too large, while a very reasonable value of 100 nm was computed for DIP.[31] A careful comparison of this approach with a more accurate hopping model[32] which employs Fermi's golden rule for the energy-transfer rates showed that the hopping model provides exciton diffusion lengths in excellent agreement (within 20%) with the well-established experimental exciton diffusion lengths of naphtalene and anthracene single crystals. However, it was shown[32] that the Marcus approach tends to underestimate L_D values. Thus, the hopping model performs rather well for exciton diffusion in DIP but strongly overestimates the L_D value of α-PTCDA. This is neither understandable from differences in the electronic characters of corresponding dimer aggregates[18] nor from the reorganization energies of these perylene derivatives which are relatively small and rather similar. Heinemeyer et al. determined a reorganization energy of 0.15 eV[33] for DIP, while Scholz and Schreiber reported values for the reorganization energy of PTCDA between 0.14 and 0.19 eV.[34] So far, all simulations completely neglected photoinduced relaxation effects which may diminish exciton diffusion in the material.

Their influence is investigated in the present work using DIP and PTCDA as model systems. Our computations use dimers as basic units. Their potential energy surfaces are computed by means of high-level ab initio approaches, while the influence of the surrounding (delocalization of the exciton, steric interactions with next neighbors in the crystal) on photo-induced relaxation processes is approximately taken into

account in a second step. A careful comparison of computed excitation energies with spectra of α-PTCDA shows that our approach is reliable. To compare with exciton hopping processes, the time scale of the photoinduced relaxation process is determined by quantum dynamical simulations of the photoexcited PTCDA cluster. For α-PTCDA crystals our model computations predict an efficient exciton trapping mechanism which explains that the experimental exciton diffusion lengths of α-PTCDA are much smaller than the result of the (trap free) hopping model. The efficiency of this trapping mechanism is a strong function of the molecular packing in the crystal. In DIP this exciton trapping is energetically unfavorable due to steric interactions with the crystal surrounding. This explains the good performance of the hopping model for this material. Our model also offers an explanation for the differences between the L_D values of DIP crystals and the corresponding thin films.

■ DESCRIPTION OF THE EMPLOYED MODEL

In a broader sense the photoinduced relaxation process predicted by our computations can be looked upon as a photoinduced exciton–phonon coupling. Such effects strongly influence absorption and emission spectra of aggregates and crystals[9,35−38] as well as charge carrier and exciton transport properties.[23,24,39−42] They are often described within the mixed Holstein–Peierls models.[43,44] The basic units of the underlying empirical Holstein–Hamiltonian are monomers. In most cases the Holstein–Hamiltonian describes excited and ground states which are coupled via the Förster term or more comprehensive expressions. Possible couplings to CT states are taken into account via separate coupling terms.[15,16,25,45,46] In most cases some or all of the occurring parameters of the model are determined by fitting of experimental data.

In the present work a complementary strategy is used which solely relies on computed properties. We employ a bottom-up strategy using dimers as basic units. Employing dimers instead of monomers as a basic unit has some advantages. Dimer computations describe the interactions between the monomers on a full quantum chemical level and provide the relative energies of all electronically excited states determining the fate of the exciton. The situation is depicted in Figure 1. In the diabatic picture, two Frenkel and two CT states emerge from the interaction of the S_1-states of the monomers. Within the
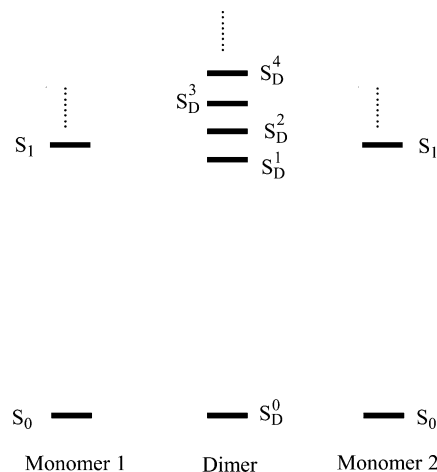
Figure 1. Correlation diagram between dimer and monomer states.

adiabatic framework used in the present approach all electronic interactions between these states are already fully taken into account. In the following the emerging states will be called $S_D^1 - S_D^4$, while the dimer ground state will be abbreviated by S_D^0. These abbreviations are used to distinguish the resulting dimer states from the monomer ones which are labeled as S_0, S_1, etc. In principle, also all higher lying states arising from the S_2 or S_3 states of the monomers can be computed, but they are not relevant for the present work.

In addition to the vertical excitation energies at the equilibrium geometry of the ground state, dimer calculations also provide potential energy surfaces of the relevant states as a function of the degrees of freedom of the two monomers with respect to each other and within themselves. We are thus in the position to describe all possible relaxation processes induced after light absorption.

The electronically excited states of interest are mixtures of Frenkel and CT states. Hence, quantum chemical methods are needed which describe their energetic position sufficiently accurate.[47,48] Multireference configuration interaction[49,50] or equation of motion coupled cluster[51] provides the necessary accuracy but are way too expensive for the given systems. The second-order approximate coupled cluster method using spin component scaling (SCS-CC2) provides an accuracy of around 0.1 eV for the energetic position of the Frenkel and CT states[47,48,52] which is sufficient. Time-dependent density functional theory (TD-DFT) which is often used to describe organic semiconductors is well suited for monomer computations. However, it is not suited for dimer computations since the energetic position of CT states are drastically underestimated.[12,53]

Using the SCS-CC2 approach, full geometry optimizations of the dimer for the respective electronic state are extremely time-consuming with the presently available computer hard- and software. Hence, the monomer geometries of PTCDA and DIP were optimized with the dispersion corrected density functional theory (DFT-D2) method[54,55] using the BLYP[56,57] functional in combination with the TZVP[58] basis set at the non-hydrogen atoms and the TZV[58] basis set at the hydrogen atoms. The ground-state potential energy surfaces as a function of the intermonomer coordinates being relevant for the given problem (see below) were computed by Møller−Plesset perturbation theory to second-order using spin-component-scaling (SCS-MP2) in combination with the resolution of identity approximation.[47,59,60] For all dimer computations we employed the SVP (split valence plus polarization) basis sets.[58,59,61−63] The analysis of the character of the excited states was performed by a method, which was proposed by Liu.[64] This approach is based on a localization of the delocalized dimer MOs to the monomers and a Löwdin's orthogonalization. After the corresponding transformation of the excited-state wave functions, the coefficients of the configurations can be used to analyze the states by their amount of CT versus Frenkel character. All quantum chemical ab initio computations were performed using the Turbomole 6.1 program package.[65]

Due to the high computational costs it was only possible to compute the potential energy surfaces (PESs) of the electronically excited states along the relevant reaction coordinates. For PTCDA, they involve the shift coordinates along the long (longitudinal shift) and short (transversal shift) molecular axis. For DIP, we used a linear path between the Franck−Condon region and the conical intersection (CI) of surfaces of S_D^1 and S_D^2.

Many investigations indicate that the exciton is delocalized across more than two monomers at the time when the excitation process happens.[66,67] Consequently, the computations of oligomers larger than dimers would be desirable, but such computations are way too costly. The dimer approach accurately takes into account all interactions between both monomers but neglects distant interactions within a stack.[68] The number of states arising from the interaction of the S_1 states of the monomers increases if the exciton is delocalized across three or even more monomers. Furthermore, the energy splitting between the energetically lowest and highest state of this manifold increases. For example, in going from a dimer to an infinite chain of monomers (homopolymer), exciton theory predicts an increase of the energy band from two times to four times the electronic coupling element.[36] The exact position of the various states can only be obtained from the computation of the respective oligomers, but the increase of the splitting between the lowest and the highest state can be approximated via Apéry's constant[69] times two. This approximates non-next interactions and corrects the Davydov splitting from the computed dimer value to the magnitude expected for stacks.[53] In our approach, Apéry's constant is employed to estimate the energetical positions of the S_D^1 and S_D^2 states. They represent kinds of the envelope states for the manifold of states which arise due to the delocalization of the exciton about several monomers. Please note that all computed transition dipole moments were taken from uncorrected dimer computations.

Since we want to describe photoinduced relaxation processes in crystals, restrictions arising from steric interactions with the environment have to be taken into account. Therefore, we embed the dimer into a large cluster of surrounding molecules (9500 atoms, 250 molecules). It comprises two layers around the inner dimer which can adapt to its motions. The second layer is surrounded by a third layer which is fixed at the crystal geometry. This system allows investigating the relaxation of the surrounding molecules in the crystal lattice as a response to a given (frozen) configuration of the central dimer. Since accurate QM approaches are too expensive to describe systems of that size, we employ a hybrid QM/MM approach instead. For the MM part in the case of α-PTCDA, we employ the AMOEBA[70] polarizable force field implemented in the TINKER program package[71] which uses distributed atomic multipoles to describe permanent electrostatic interactions. The atom-centered multipoles (up to quadrupoles) were calculated with the distributed multipole analysis (GDMA) program.[72,73] In addition to permanent electrostatic interactions, damped induced dipoles at each atomic center are used for explicit treatment of many-body polarization effects (nonpairwise additive). To take the intramolecular degrees of freedom in the PTCDA and DIP molecules correctly into account, we have parametrized the corresponding force field parameters based on the monomer calculations to reproduce the B3LYP/cc-pVDZ optimized geometries[74] and the corresponding Hessian matrix (especially low-frequency modes <200 cm^{-1}) as described in ref 75. To reproduce the crystal structure of DIP, it was necessary to develop a completely new force field. For this we used the same approach as described recently for polycyclic aromatic compounds.[76] Since the new force field includes explicitly the short-range charge penetration contribution,[77] the van der Waals parameters have to be reparameterized. To this end, all terms were fitted to the corresponding terms calculated using symmetry-adapted perturbation theory (SAPT). As a consequence, a more balanced force field is obtained.[78]
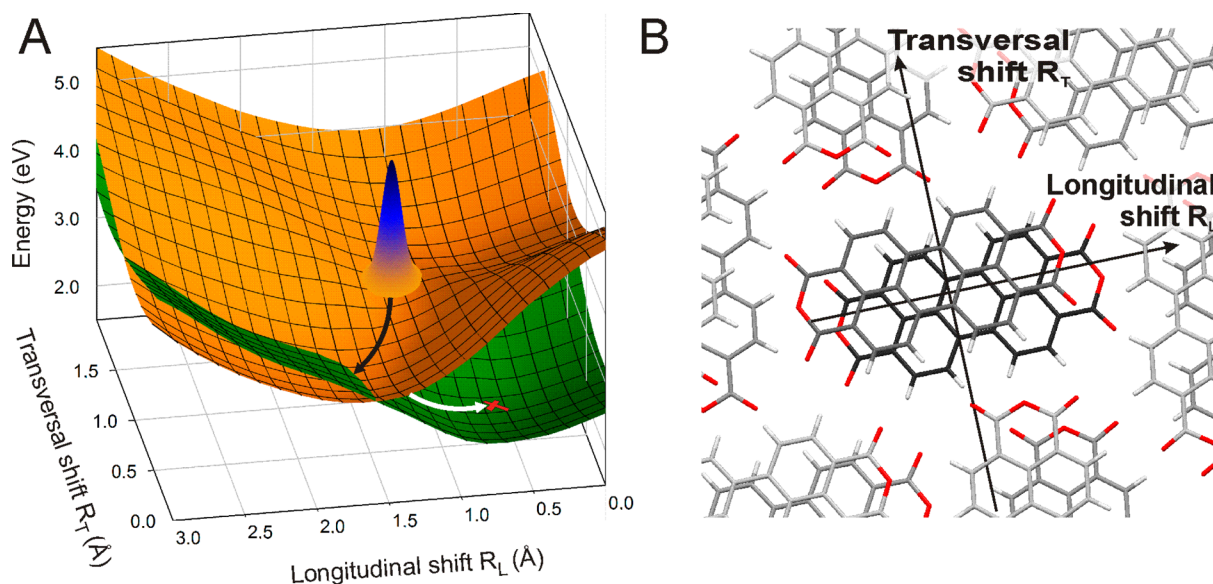
Figure 2. Molecular motion after photoexcitation in α-PTCDA. (A) Relevant potential energy surfaces for α-PTCDA and (B) geometrical arrangement of α-PTCDA molecules in the crystal structure.

Within this hybrid QM/MM approach the ground-state energy of the whole system is calculated in the subtractive scheme (mechanical embedding):

$$E(\text{QM/MM}) = E_{\text{dimer}}(\text{QM}) + E_{\text{full-system}}(\text{MM}) - E_{\text{dimer}}(\text{MM})$$

where $E_{\text{dimer}}(X)$ is the dimer intermolecular energy calculated at the respective level (X = QM or MM). $E(\text{MM})$ is the energy of the whole cluster geometrically optimized by the specially developed force fields. Dimer excitation energies (corrected with Apéry's constant) are added to the ground-state energy $E(\text{QM/MM})$. Our mechanically embedded QM/MM approach includes all steric interactions between the dimer and the environment. It also allows the adaption of the surrounding to photoinduced motions of the dimer. Additional polarization effects due to the crystal environment are reproduced only partially, but they are expected to be small.[79]

In order to estimate the time scales of the proposed trapping mechanism, quantum dynamical simulations of the photo-excited PTCDA cluster are performed using grid-based methods. Here, the two-dimensional potential energy surface of the initially populated S_D^2 state serves as potential energy term in the Hamiltonian, while the kinetic energy operator has to be derived not only in the degrees of freedom corresponding to the longitudinal and transversal linear shifts of the two central monomers but also in the nonlinear motion of the geometrically optimized surrounding crystal. The complex form of an exact kinetic energy operator in curvilinear coordinates[80,81] is drastically simplified by assuming stepwise linear motions from one geometry j defined by the coordinates $\{\vec{x}_{\alpha,j}\}$, where α runs over all 9500 cluster atoms, to the vicinal geometry $j + 1$. Along this pathway described by a reaction coordinate $q \in [0,1]$, the geometry can be written as

$$\vec{x}_{\alpha,[j,j+1]}(q) = \vec{x}_{\alpha,j} + q \cdot (\vec{x}_{\alpha,j+1} - \vec{x}_{\alpha,j})$$

Within this linear approximation, the system's inertia can be understood as an effective mass[22] determined by

$$m_{(j,j+1)} = \sum_{\alpha} m_{\alpha} |\vec{x}_{\alpha,j+1} - \vec{x}_{\alpha,j}|^2$$

where m_{α} is the mass of atom α. Note that in our two-dimensional scheme $j + 1$ refers either to a vicinal geometry in the direction of the transversal shift or to one in the longitudinal direction. Thus, different effective masses, $m_{L,j,j+1}$ and $m_{T,j,j+1}$, are obtained over the two-dimensional surface for each geometry pair $(j, j + 1)$ parallel to the axes (see SI for further details).

As these effective masses essentially reflect the linear motion of the central dimer and do not vary substantially along the reaction coordinates, we use averaged values, $m_L = 1.59 \times 10^6$ hartree^{-1} and $m_T = 1.80 \times 10^6$ hartree^{-1}. This results in a continuous expression for the two-dimensional kinetic energy operator:

$$T(q_L, q_T) = \frac{-1}{2m_L}\frac{\partial^2}{\partial q_L^2} + \frac{-1}{2m_T}\frac{\partial^2}{\partial q_T^2}$$

The variables q_L and q_T are dimensionless reaction coordinates for collective motions of all cluster atoms. They are numerically defined such that one step of $\Delta_{q_{L,T}} = 1$ represents a shift of 1 Å of the central monomers with respect to each other. Therefore, the dimensionless numerical value of q_L (q_T) coincides with the monomer shift R_L (R_T) given in Å.

Afterward, the quantum dynamical wave packet propagation is performed by integrating the time-dependent Schrödinger equation numerically employing the split-operator method.[82] The vibrational ground state of the state S_D^0, determined via imaginary time propagation,[83] provides the initial wave packet, which is placed in the Franck−Condon region of the S_D^2 state resembling photoabsorption. The wave packet is propagated until passing the seam of the CI as illustrated in Figure 2a, black arrow.

RESULTS AND DISCUSSION

Characterization of Photoinduced Processes in α-PTCDA. The potential energy surfaces of the S_D^1 and S_D^2 states as a function of the transversal (R_T) and longitudinal shift (R_L) are depicted in Figure 2. Both states possess predominantly Frenkel character (Figure 3). Information about the adiabatic states S_D^3 and S_D^4, which have mainly CT character are omitted
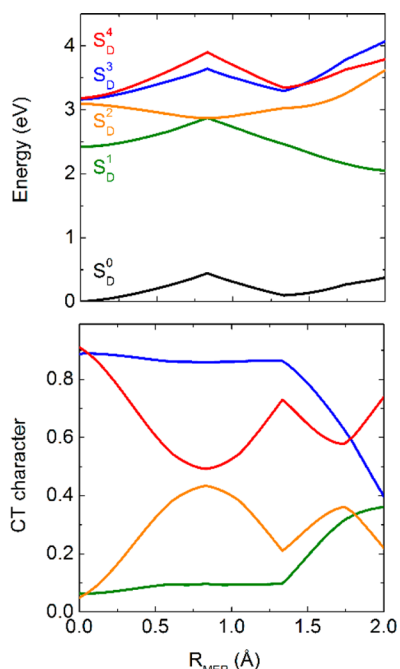
Figure 3. Cut through the PESs of α-PTCDA along the minimal energy path (MEP, see Figure 2a). The abscissa refers to the traveled distance from the Franck−Condon region ($R_{MEP} = 0.0$ Å) via the conical intersection ($R_{MEP} = 0.83$ Å) to the energy minimum of the S_D^1 state ($R_{MEP} = 2.0$ Å). The lower plot quantifies the respective contributions of the diabatic CT states to the overall wave function.[61]

for clarity as they are energetically well separated for the crystal geometry discussed here (Figure 3). The vertical excitation energies of the S_D^1 and S_D^2 states are 2.4 and 3.1 eV, respectively. For the upper state (S_D^2) we predict a transition dipole moment of about 1.15 au, while the transition dipole moment of the S_D^1 state vanishes due to the high symmetry of the dimer. The Franck−Condon region of the S_D^2 state ($R_L = 1.19$ Å; $R_T = 1.05$ Å) is indicated by a wave packet (Figure 2a, orange) which represents the initial excited-state probability distribution prepared by a δ-pulse excitation to the S_D^2. The potential gradient induces a barrier-free intermolecular motion (black arrow), which guides the system toward a CI[84] with the lower lying S_D^1 state (Figure 2a, green). If the exciton crosses over to the S_D^1 state it can further relax to the local minimum (white arrow, red cross) of the S_D^1 state at $R_L = 0.64$ Å; $R_T = 0.49$ Å. At that geometrical arrangement the energy difference between the S_D^1 and the ground state decreases to 1.5 eV since the ground state is destabilized (0.5 eV relative to the global minimum), while the S_D^1 state is stabilized with respect to the CI by about 0.4 eV.

The time required to reach the CI was estimated by a wave packet propagation on the two-dimensional potential energy surfaces (PES) of the S_D^2 state from the Franck−Condon region. The path taken by the wave packet is indicated by the black arrow in Figure 2a. The computations predict that the CI is reached within 400−500 fs after photoexcitation. This is slightly shorter or in the same time regime as usual exciton-transfer times (10^3–10^6 fs).[85] As wave packets are known to change instantaneously between electronic states upon reaching a CI,[84] our computations reveal a very efficient photorelaxation process from the Franck−Condon region of the S_D^2 state to the minimum of the S_D^1 state for α-PTCDA crystals or aggregates. Please note that if the S_D^1 is directly populated through

photoabsorption the corresponding gradient also directs the exciton to the same minimum (Figure 2A red cross).

Before we interpret our results with respect to exciton diffusion we will critically investigate the accuracy of our approach by comparisons to the experimental data provided by Bulovic et al.,[86] Alonso et al.,[87] and Engel et al.[88] Bulovic et al. published an absorption spectrum of a 100 nm thick PTCDA film which exhibits three bands. The energetically lowest band is quite weak and narrow (0.2−0.3 eV) and has a maximum at about 2.2 eV. A broader and considerably more intense peak is found between 2.4 and 2.9 eV with a band maximum at 2.7 eV. The absorption spectra measured by Alonso et al.[87] resembles the one given by Bulovic et al.[86] By measuring parallel and perpendicular to the *b*-axis Alonso et al. could indicate that both peaks represent two states resulting from Davydov splitting, i.e., the underlying states result from the interaction of monomeric S_1 states. Engel et al.[88] measured the absorption spectrum up to 2.6 eV. They also find a weaker band with a maximum between 2.2 and 2.3 eV. At about 2.4 eV another band was observed which does not reach its maximum up to 2.6 eV. Bulovic et al. and Engel et al. also presented emission spectra. The emission spectra provided by Bulovic et al. possess one structureless band which starts somewhat below 1.5 eV and has its peak maximum at about 1.7 eV. The emission spectrum given by Engel et al. was measured at 10 K. The most intense peak maximum is at about 1.8 eV, while two considerably lower peaks are found at about 1.6 and 1.9 eV.

Our computed vertical excitation energies nicely agree with the experimental absorption spectra. The lower lying S_D^1 state which represents a kind of envelope state is computed to lie at about 2.4 eV. This is slightly higher than the measured peak maximum of the lower peak (2.2 eV) but lies within the error bars expected for our approach. The S_D^2 state which also represents a kind of envelope state of the expected state manifold is predicted to be at about 3.1 eV. This is slightly higher than the upper band edge of the higher peak which is found at 2.9−3.0 eV. According to the considerations about the manifold of electronic states arising from the delocalization of the exciton, the broadening of both peaks should not only result from vibronic interactions. Electronic states arising from the delocalization of the exciton over larger aggregates than dimers should also contribute to the broadness of the observed spectrum. Beside the energetical positions of the bands, also the intensity ratio of both bands is convincingly reproduced by our computations. The dimer calculations predict a vanishing transition dipole for the lower state of the dimer, but a weak intensity is expected due to the delocalization of the exciton and the influence of the crystal environment.

The calculated results are also in good correspondence with the emission spectra. Obviously, the experiments of Bulovic et al. and Engel et al. provide very similar emission spectra although different excitation pulses were used. The excitation pulse of Engel et al. was centered at 2.22 eV to populate the lowest vibronic state. Bulovic et al. used pump energies of 2.72 and 2.05 eV and found no significant changes in the thin-film fluorescence spectra. At the first glance this is astonishing since two different states should be populated by the different pump pulses. The pump pulses at 2.22 and 2.05 eV should only populate the lower state (absorption band with maximum at 2.2 eV), while the pulse at 2.72 eV should populate the upper state connected with the absorption band with the peak at 2.7 eV. Please note that both peaks are assigned to different states according to not only our calculation but also to the assignment

of Bulovic et al. Our computations readily explain why the population of two different states leads to the same emission spectra. If the higher excitation pulse is used the higher lying states are populated, but due to the photoinduced relaxation process described above the exciton is rapidly transferred to the S_D^1 state. Our computations only provide information about the envelope states but, since they cross in the CI it can be expected that all other electronic states show a similar behavior. If using the pump pulses with the lower energy, only the S_D^1 state is populated, but also in this case the exciton moves to the same minimum of the S_D^1 state (see Figure S1). For the minimum of the computed S_D^1 state we calculated an emission energy of 1.5 eV which again nicely agrees with the position of the measured emission peaks. The long lifetime of the lower state ($\approx$ 11 ns)[86] is also in perfect agreement with the low transition probability computed for the S_D^1 state. The comparison strongly supports the reliability of our approach especially since we do not include any fitting procedure to available experimental results.

After discussing the reliability of our approach we can turn to the question how the photoinduced relaxation processes influence exciton diffusion. We already mentioned that calculations based on the Marcus approach predict an exciton diffusion length of about 160 nm for PTCDA, while experimentally a value of only 22 nm was observed. We also pointed out that the deviation between experiment and theory should be even larger since the Marcus-based approach tends to underestimate exciton diffusion lengths. Within Marcus' approach the hopping rate is given as

$$v_{ij} = \frac{V_{ij}^2}{\hbar} \sqrt{\frac{\pi}{\lambda k_B T}} \exp\left[-\frac{\lambda}{4 k_B T}\right]$$

where V_{ij} is the electronic coupling parameter, λ is the reorganization energy, T is the temperature, and k_B is the Boltzmann constant. The reorganization energy is the difference between the excitation energy of the acceptor and the emission energy of the donor.

$$\lambda(R_{MEP}) = \Delta E_{acceptor}^{absorption} - \Delta E_{donor}^{emission}(R_{MEP})$$

Due to the relaxation processes (Figure 4) taking place at the donor the relaxation energy depends on R_{MEP} (Figure 3).
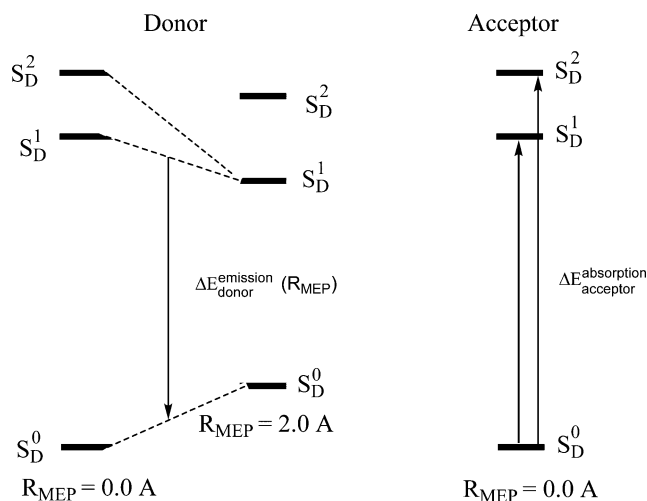
Figure 4. Sketch to explain the increase of the relaxation energy λ along the relaxation process. For more details see text and Figure 3

Within Förster's approach the electronic coupling parameter V_{ij} is proportional to the product of the transition dipole moments of donor and acceptor.

Let us first discuss the possibility that the exciton populates the S_D^2 state and hops to the S_D^2 state of an acceptor. In this situation the electronic coupling parameter V_{ij} is large since the S_D^2 state has a high transition dipole moment. For the hop between the S_D^2 states of donor and acceptor the excitation energy of the acceptor is given by the vertical excitation energy of the S_D^2 state because the acceptor chromophore is in the global minimum of the ground state (Figure 4 right-hand side). The emission energy of the donor, however, decreases steadily along the relaxation process in which the exciton moves along the minimum energy path (MEP) across the CI to the minimum of the S_D^1 state. The decrease results from the stabilization in the excited state and the accompanied destabilization in the ground state. As a consequence the reorganization energy rises very fast because the excitation energy of the acceptor remains constant. If the minimum of the S_D^1 state is reached, the reorganization energy amounts to 1.6 eV. This is much higher than the relaxation energy determined for the monomer relaxation which amounts to 0.38 eV. An increased reorganization energy which enters the Marcus' equation exponentially causes the hopping rate V_{ij} to decrease considerably along the relaxation path.

The exciton diffusion length L_D, of course, only decreases if the energy released from the relaxation is dissipated to the environment. If it stays in the system, e.g., as vibronic excess energy, the exciton hopping can still take place. Hence, for the shortening of L_D it is important how fast the energy is dissipated to the environment. Various experimental estimates indicate that the dissipation of energy proceeds on a time scale of 100−1000 fs.[89,90] Taking into account that the motion to the conical intersections takes about 500 fs the assumption that 25−50% of the excess energy gets dissipated to the environment seems to be justified. To get rough estimates of the resulting influence we simulated the exciton diffusion lengths as described in ref 31 assuming that only 25% (0.4 eV) or 50% (0.8 eV) of the total excess energy of 1.6 eV are dissipated. The rest of the parameters were approximated by their monomeric counterparts. If only 0.4 eV are dissipated (25%) the computed L_D value already shrinks from about 160 to 18 nm. If 50% of the excess energy (0.8 eV) are dissipated a value of L_D = 2 nm is computed.

If the exciton finally reaches the CI and is transferred to the S_D^1 state the situation becomes even less favorable. After crossing the CI the donor emission takes place from the S_D^1 state which has a much smaller transition dipole moment than the S_D^2 state, i.e., the electronic coupling parameter (V_{ij}) also decreases drastically. After the exciton has reached the minimum of the S_D^1 state it can still hop to the S_D^1 state of the acceptor, but as will be explained below, this process is also strongly hampered. Please note that after emission to the ground state the system will relax to the crystal structure, i.e., the photoinduced distortion is only temporally. As a consequence possible acceptors are always in the geometry of the ground state.

If the manifold of states resulting from the delocalization of the exciton across several monomers is taken into account the situation becomes slightly more favorable since the computed S_D^2 represents a kind of envelope state. This leads to lower reorganization energies since states within the manifold of states being lower in energy than the computed S_D^2 can be

populated. Nevertheless, the basic picture remains. Since the relaxation process to the CI is very fast, the relaxation process described above strongly hampers the exciton hopping, i.e., the transfer to the S_D^1 state can be looked upon as a kind of trap.

The absorption peak at about 2.2 eV indicates that also lower states of the manifold of states are populated. Hence, we have to consider exciton hopping starting from such states, which in our case are modeled by the S_D^1 state. Within Marcus' theory a transfer to higher lying states of the manifold, which in our approach are represented by the S_D^2 state, will not take place due to the high accompanied reorganization energies. A transfer to the S_D^1 state of the acceptor is possible, but the hopping rate is expected to be small due to two reasons. First, the electronic coupling parameter is smaller than for the $S_D^2 \rightarrow S_D^2$ transfer because the transition dipole moment of the S_D^1 state is much smaller than the corresponding values for the S_D^2 state. Furthermore, due to the possible relaxation from $R_{MEP} = 0$ Å to the minimum of the S_D^1 state (see SI for more details) also for the $S_D^1 \rightarrow S_D^1$ transfer the reorganization energy amounts to 0.9 eV after complete relaxation. Reducing the coupling parameter of our simulation to a quarter of the value taken for the $S_D^2 \rightarrow S_D^2$ transfer and again assuming that only about 25% of the excess energy is dissipated to the environment, the simulation predicts $L_D = 12$ nm. This indicates that the relaxation processes also hamper the $S_D^1 \rightarrow S_D^1$ exciton diffusion.
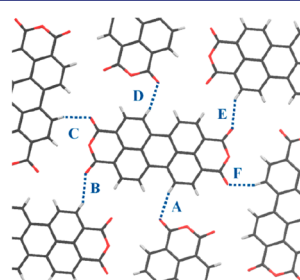
Summarizing our consideration, the relaxation processes after photoexcitation predicted for the PTCDA crystal considerably hampers all possible exciton hopping processes, which explains the short measured exciton diffusion length. This mechanism differs from the one suggested by Scholes et al.[23] and Spano et al.[24] which refers the fast confinement of the delocalized exciton to only a few monomers. This process which is already finished before the present trapping mechanism takes place does not lead to an efficient trapping since the exciton can still move through the crystal by hopping. Our mechanism, for which the trapping occurs through population transfer between both predominantly Frenkel states, also deviates from the one suggested by Forrest et al.[86] They predicted that the trapping happens through transfer from Frenkel to CT states. In our model, through the mixing (see below) CT states only play an indirect role since they are too high in energy. Finally, it also differs from the trapping mechanism we suggested for PBI aggregates in which the monomers are twisted with respect to each other. Here, CT states play the crucial role of a doorway state while they do not seem to be involved in the present mechanism. Taking into account that the electronic structures of both PBI and PTCDA monomers bear strong resemblance,[18] this comparison indicates that the respective trapping mechanism strongly depends on the mutual orientation of the monomers in the given aggregate rather than on their individual electronic characteristics.

Recently, Athanasopoulos et al.[91] discussed a trapping mechanism for conjugated polymers. In a simulation of the energy diffusion dynamics in a polyindenofluorene conjugated polymer they only obtained agreement between computed and measured exciton diffusion lengths if they postulated ordered regions which possess higher densities of states. These regions act as traps since the relaxation to the bottom of the aggregate exciton band, which is dark for H-aggregates, is assumed to be much faster at room temperature than the exciton transfer. Our computations offer a possible atomistic picture for such traps. They also indicate that the ordered regions do not have to be

spatially extended, since efficient trapping processes seem to occur even for dimerized monomeric units.

Figure 3 and Figure 5 offer explanations why the CI between S_D^1 and S_D^2 exists. From Figure 3 reasons for the opposite

distance	FC	CI
A	2.39	2.24
B	2.49	2.36
C	2.39	2.27
D	2.39	2.50
E	2.49	2.63
F	2.39	2.45

Figure 5. Shortest intermolecular distances (in Å) for α-PTCDA at the Franck−Condon (FC) region and the CI with the optically dark S1 state. The distances are indicated on the right-hand side.

curvatures of S_D^1 and S_D^2 leading to the CI become clear. The upper part shows the potential energy curves along the MEP of the S_D^1 state. The abscissa denotes the traveled distance R_{MEP} from the Franck−Condon region ($R_{MEP} = 0.0$ Å) of the S_D^2 state to the CI ($R_{MEP} = 0.83$ Å; Figure 2A black arrow) and then the distance along the subsequent relaxation on the S_D^1 ($R_{MEP} = 2.0$ Å; Figure 2A white arrow). Please note that this path is completely different from the relaxation path from the Franck−Condon region of the S_D^1 state to its own minimum, which is barrier-free. The lower plot shows the variation in the amount of CT character for the various states. Figure 3 demonstrates that only the initially populated S_D^2 state is stabilized between the Franck−Condon region ($R_{MEP} = 0$) and the CI ($R_{MEP} = 0.83$ Å). All other states, including the ground state are destabilized. The destabilizations result from repulsive steric interactions between the dimer molecules and the molecules of the crystal environment which arise due to the photoinduced relaxation on the S_D^2 state. The motions are indicated in Figure 5. While distance A (see Figure 5) decreases from 2.39 to 2.24 Å, the distance D increases from 2.39 to 2.50 Å. Both distances are indicators for the transversal shifts of the photoinduced motion in the S_D^2 state. Distance C is mainly affected by the longitudinal shift. It shrinks for the motion from the Franck−Condon region to the CI (from 2.39 to 2.27 Å).

Corresponding repulsive interactions can also be assumed for the S_D^2 state. However, they are overcompensated by strong electronic interactions with the S_D^4 state which are reflected in the variations of the CT characters of both states (lower part of Figure 3, orange and red curves). For distance $R_{MEP} = 0$, the S_D^2 state has 95% Frenkel and 5% CT character. The opposite ratio is found for the S_D^4 state. Along the relaxation path the CT character of the S_D^2 state increases considerably, while that of the S_D^4 state decreases by the same amount. This mixing is allowed because both states belong to the same irreducible representation (^1A_u). Due to these interactions the corresponding potential energy surfaces repel each other leading to a lowering of the S_D^2 state by 0.21 eV, whereas the energy of the S_D^4 state increases by 0.72 eV. The asymmetrical splitting arises since the steric interactions discussed above decrease the stabilization of the S_D^2 state but increase the destabilization of the S_D^4 state. These interactions are also indicated by the fact that the S_D^4 state is more destabilized than the S_D^3 state (0.49 eV). The S_D^3 state can interact with the S_D^1 state (both ^1A_g). However, the weak variations in their electronic characters
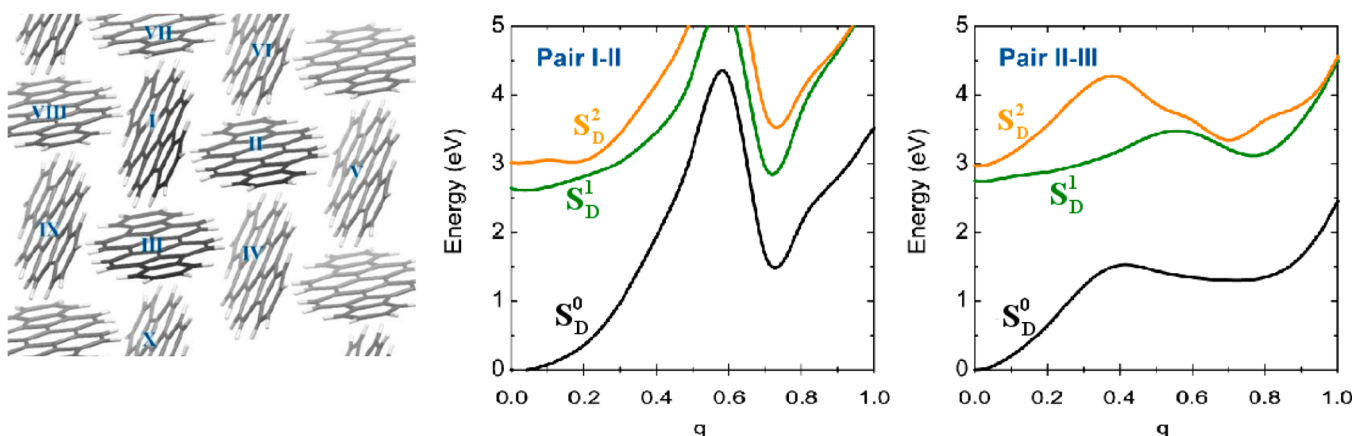
Figure 6. Arrangement of DIP molecules in the crystal (left). Potential energy curves for the paths from the Franck–Condon region ($q = 0.0$) toward the CI ($q = 1.0$) of the respective monomer pairs (middle: I–II; right: II–III) with the steric restrictions imposed by the crystal packing taken into account.

indicate that this interaction is rather small. As a consequence, interactions with the crystal environment lead to a destabilization of both states.

Characterization of Trapping Processes in DIP. In the crystal structure of DIP two symmetrically different dimers (I–II and II–III) coexist (see Figure 6). The dimers I–III and I–II are equivalent due to the space group of the crystal ($P2_1/a$). In line with the very similar electronic structure of PTCDA and DIP,[16] the CT states are again well separated from the optical active Frenkel state S_D^2 in DIP. For the DIP dimer we find similar mixture ratios for the states as discussed for the PTCDA dimer. Also the CI between the S_D^1 and S_D^2 states is found at a very similar dimer alignment as for PTCDA. To investigate whether this CI can be reached effectively after excitation in the crystal, we introduce a dimensionless reaction coordinate q which linearly relates the Franck–Condon region of DIP ($q = 0$) with the CI ($q = 1$) for both dimers of the unit cell. The corresponding energy profiles of S_D^1 and S_D^2 are depicted in Figure 6. Of course we have to consider the energy profiles for the two geometrically distinct dimers of the unit cell. For the Franck–Condon region ($q = 0$) the computed excitation energies are 2.7 and 3.0 eV, respectively. Again the transition dipole moment for the upper state is quite large (1.59 au). For the lower one the computations predict a vanishing transition dipole moment. The energy profile for the S_D^2 state (orange curves) computed for the I–II dimer possesses a barrier of 3.29 eV, whereas a barrier of 1.58 eV is computed for the process starting from the II–III dimer orientation. The barriers result from the strong steric repulsions to the next neighbors within the crystal (for a list of the shortest intermolecular distances for $q = 0$ and $q = 0.4$, see Table 1). The barriers strongly hinder a motion to the CI after excitation so that relaxation processes involving radiationless transitions cannot take place for both pairs. For both pairs the Franck–Condon region even represents a local minimum for the populated S_D^2 state. As a consequence, the monomers essentially stick to their positions. Since both energy profiles resemble each other, the same situation is predicted for the S_D^1 state.

Our calculations indicate a strong confinement of the DIP molecules due to the crystal environment. The question arises if relaxation processes become possible if the restrictions are lifted. This situation, without any steric hindrance, was mimicked by dimer calculations. Figure 7 shows the energy profiles from the Franck–Condon region of the crystal

Table 1. Shortest Intermolecular Distances (in Å) for DIP at the Franck–Condon (FC; $q = 0$) Region and at $q = 0.4$ for Both Dimers[a]

distance	FC	$q = 0.4$ (I–II)	$q = 0.4$ (II–III)
I–II	2.86	2.22	2.80
I–III	2.86	2.78	2.90
I–VI	2.86	2.26	3.00
I–VII	2.86	2.52	2.77
I–VIII	2.86	2.93	2.78
I-IX	2.86	2.86	3.40
II–III	2.86	2.52	3.12
II–IV	2.86	3.08	4.70
II–V	2.86	3.12	3.05
II–VI	2.86	2.37	2.77
III–IV	2.86	2.84	2.56
III–IX	2.86	3.26	3.29
III–X	2.86	2.92	2.6

[a]For the labeling of monomers see Figure 6.
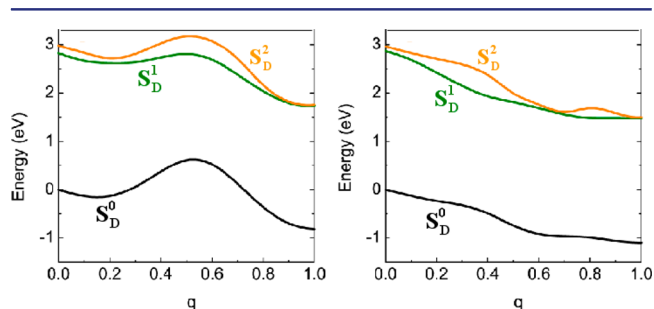
Figure 7. Potential energy curves of DIP dimers for the paths from the Franck–Condon region of the respective pairs ($q = 0.0$) toward the CI ($q = 1.0$) of the monomer pairs (left: I–II; right: II–III) without steric restrictions due to neighboring molecules.

orientation ($q = 0$) to the CI between the S_D^1 and S_D^2 states. The CI ($q = 1$) is now considerably lower in energy than the Franck–Condon region of the crystal structure. For dimer I–II, we predict a barrier of only 0.19 eV. For dimer II–III, we find even no barrier. This energy profile steadily decreases with q so that after excitation the system can very efficiently relax to the configuration with $q = 1$, where the exciton gets trapped. Please note that not only the excited states are stabilized but also the ground state stabilizes considerably. This indicates that the

geometrical orientation between monomers will change drastically once the restrictions arising from the crystal environment are lifted. This situation might be present at grain boundaries or defects induced during crystal growth or thin-film formation. For the relaxed structure we predict smaller excitation energies ($\approx$2.6 eV) than for the crystal structure arrangement. Since for the relaxed structures the molecules no longer form stacks, Apéry's factor was neglected in this case. For $q = 1$ the transition dipole to the slightly lower state is predicted to be 0.7 au.

Comparisons with available experimental data for thin films are difficult for DIP. The excitation energies obtained for the crystal structure cannot be compared with experimental data of thin films, since our computations predict a strong reorientation of the DIP molecules if the crystal restrictions are lifted. Further complications arise because the individual molecular positions in thin films are only known on a temporal and spatial average. This represents a problem because our computations indicate that the excitation energies strongly depend on the actual orientation of the molecules. Actually, the computed excitation energies obtained for the relaxed structure ($\approx$2.6 eV) fit considerably better than the excitation energy obtained for the bright state at the crystal structure (3.0 eV). Further computations are underway, but they are beyond the scope of the present paper which concentrates on the relaxation processes within crystals.

The model obtained from our computations for relaxation processes after photoexcitation in the DIP crystal differs completely from the corresponding picture obtained for α-PTCDA. In the latter, exciton diffusion is strongly hampered since the fast relaxation processes leads to very high reorganization energies. For DIP our computations predict that after excitation the molecules are confined to their ground-state orientations. Hence, much smaller reorganization energies are expected so that no hampering of the exciton diffusion is expected. This is predicted for $S_D^2 \rightarrow S_D^2$ and $S_D^1 \rightarrow S_D^1$ hops between donor and acceptor. This explains the long exciton diffusion lengths measured for DIP single crystalline samples.[29,30,92] For polycrystalline thin films comprising grain boundaries or crystals containing defects our computations provide another picture since the relaxation processes now become possible once the crystal restrictions are lifted. This explains the considerably shorter exciton diffusion length found for thin films consisting of smaller crystallites or being even structurally disordered. It is also in line with recent experiments. They indicate that very efficient exciton diffusion is found within DIP crystalline domains, whereas the interdomain transport is strongly hampered by activation barriers.[92]

A comparison between the situations found for α-PTCDA and DIP and also in other perylene-based dyes[12,93] shows that exciton trapping through conical intersections between the two predominantly Frenkel states are quite likely at least for H-aggregates of perylene-based compounds. The CIs result from the high density of states, the strong nonadiabatic interaction between the various states, and their strong dependence on the mutual orientations of the monomers. Since most organic functional materials with extended π-conjugated system have similar properties, we assume that comparable trapping processes will also be present in these compounds. Our assumption is supported by the study of Athanasopoulos et al.[91] discussed above.

Our computations for DIP, however, indicate that exciton trapping can be diminished if the packing motifs of the constituting monomers hinder intermolecular motions toward CIs. This can be achieved either by the crystal packing as for DIP or by bulky substituents, as already indicated experimentally.[27,28] Alternatively, our computations predict that the present trapping mechanism should not take place in crystals with relatively large distances between adjacent molecules. This results because the CI being responsible for the fast transfer to the trapping state (as in the case of α-PTCDA) vanishes for monomer distances exceeding 3.8 Å. Packing motifs with large distances between adjacent molecules or nonface-to-face orientations such as in the herringbone arrangement, should also lead to larger L_D, as shown, e.g., for oligoacene single crystals, e.g. anthracene.[45]

For J-aggregates our model also predicts higher L_D values since in contrast to H-aggregates the lowest excited state is populated. For the development of efficient devices it has to be taken into account, however, that large distances between adjacent molecules hamper the charge carrier transfer taking place after the exciton dissociation.

SUMMARY AND CONCLUSIONS

Based on a hybrid approach which combines high-level ab initio calculations of PES of dimers with more approximate considerations of the crystal environment and subsequent quantum dynamical simulations, we present a plausible relaxation process from photoexcited states which explains the short exciton diffusion lengths (L_D) of crystalline α-PTCDA as well as the long L_D measured for crystalline DIP. According to our predictions, the short diffusion lengths found for PTCDA are caused by ultrafast relaxation processes after photoexcitation guiding excitons which populate the S_D^2 state to a conical intersection (CI) with the lower lying S_D^1 state. Quantum dynamical simulations on the computed PES predict that it takes only about 400−500 fs to reach the CI. After the population transfer to the lower-lying S_D^1 state through the conical intersection, the system further relaxes to a nearby local minimum of the S_D^1 state. A strong hampering of the exciton diffusion occurs since the exciton loses a considerable amount of energy during the relaxation process. This leads to a fast increase of the reorganization energy so that the hopping rates are considerably lowered. After reaching the minimum of the S_D^1 state the exciton may still hop to the S_D^1 state of the acceptor, but for this process we predict quite large reorganization energies. Furthermore, the hopping rate is further reduced due to the nearly vanishing oscillator strength for the S_D^1 emission. Possible $S_D^1 \rightarrow S_D^1$ hops taken place after the direct population of the S_D^1 state are hampered due to similar reasons. Taking into account that usual exciton-transfer times range from 10^3 to 10^6 fs, our model suggests that the exciton trapping is rather efficient, limiting exciton diffusion to just a few hops.

Crystalline DIP also possesses the corresponding CI, but the relaxation process necessary to reach the CI is blocked by steric hindrances resulting from the crystal packing. The resulting barriers even confine the system to the geometry of the ground state which additionally leads to a very efficient exciton transfer. Nevertheless, our computations show that as soon as these steric restrictions are lifted (e.g., at grain boundaries or defects) a similar trapping process as discussed for α-PTCDA can take place very efficiently. This prediction is in line with the measured differences in the L_D values of single crystalline and polycrystalline DIP.

■ ASSOCIATED CONTENT

Ⓢ Supporting Information

Details of the quantum dynamical simulation together with the potential energy surface of the S_D^1 state and the Cartesian coordinates of relevant DIP and PTCDA dimers are given. This material is available free of charge via the Internet at http://pubs.acs.org/.

■ AUTHOR INFORMATION

Corresponding Author

bernd.engels@mail.uni-wuerzburg.de

Present Addresses

‖Institut für Physikalische and Theoretische Chemie, Universität Tübingen, Auf der Morgenstelle 18, 72076 Tübingen, Germany.

⊥Laboratoire Collisions Agrégats Réactivité - IRSAMC (UMR 5589), Université Paul Sabatier, 118 route de Narbonne, 31062 Toulouse Cedex 09, France.

#Institut für Physikalische Chemie, Universität Mainz, Duesbergweg 10-14, 55128 Mainz, Germany.

Notes

The authors declare no competing financial interest.

■ ACKNOWLEDGMENTS

■ REFERENCES

(1) Peumans, P.; Yakimov, A.; Forrest, S. R. *J. Appl. Phys.* **2003**, *93*, 3693; Erratum *J. Appl. Phys.* **2004**, *95*, 2938.

(2) Bakulin, A. A.; Rao, A.; Pavelyev, V. G.; van Loosdrecht, P. H. M.; Pshenichnikov, M. S.; Niedzialek, D.; Cornil, J.; Beljonne, D.; Friend, R. H. *Science* **2012**, *335*, 1340.

(3) Heremans, P.; Cheyns, D.; Rand, B. P. *Acc. Chem. Res.* **2009**, *42*, 1740.

(4) Schmidt-Mende, L.; Fechtenkötter, A.; Müllen, K.; Moons, E.; Friend, R. H.; MacKenzie, J. D. *Science* **2001**, *293*, 1119.

(5) Deibel, C.; Dyakonov, V. *Rep. Prog. Phys.* **2010**, *73*, 096401.

(6) Deibel, C.; Mack, D.; Gorenflot, J.; Schöll, A.; Krause, S.; Reinert, F.; Rauh, D.; Dyakonov, V. *Phys. Rev. B* **2010**, *81*, 085202.

(7) Beljonne, D.; Cornil, J.; Muccioli, L.; Zannoni, C.; Brédas, J.-L.; Castet, F. *J. Chem. Mater.* **2011**, *23*, 591.

(8) Collini, E.; Scholes, G. D. *Science* **2009**, *323*, 369.

(9) Brédas, J.-L.; Norton, J. E.; Cornil, J.; Coropceanu, V. *Acc. Chem. Res.* **2009**, *42*, 1691.

(10) West, B. A.; Womick, J. M.; McNeil, L. E.; Tan, K. J.; Moran, A. M. *J. Phys. Chem. B* **2011**, *115*, 5157.

(11) Forrest, S. R. *Chem. Rev.* **1997**, *97*, 1793.

(12) Liu, W.; Settels, V.; Harbach, P. H.; Dreuw, A.; Fink, R. F.; Engels, B. *J. Comput. Chem.* **2011**, *32*, 1971.

(13) Giaimo, J. M.; Lockard, J. V.; Sinks, L. E.; Scott, A. M.; Wilson, T. M.; Wasielewski, M. R. *J. Phys. Chem. A* **2008**, *112*, 2322.

(14) Hippius, C.; van Stokkum, I. H. M.; Zangrando, E.; Williams, R. M.; Wykes, M.; Beljonne, D.; Würthner, F. *J. Phys. Chem. C* **2008**, *112*, 14626.

(15) Gisslén, L.; Scholz, R. *Phys. Rev. B* **2009**, *80*, 115309.

(16) Hoffmann, M.; Schmidt, K.; Fritz, T.; Hasche, T.; Agranovich, V. M.; Leo, K. *Chem. Phys.* **2000**, *258*, 73.

(17) Fink, R. F.; Seibt, J.; Engel, V.; Renz, M.; Kaupp, M.; Lochbrunner, S.; Zhao, H. M.; Pfister, J.; Würthner, F.; Engels, B. *J. Am. Chem. Soc.* **2008**, *130*, 12858.

(18) Settels, V.; Liu, W.; Pflaum, J.; Fink, R. F.; Engels, B. *J. Comput. Chem.* **2012**, *33*, 1544.

(19) Fückel, B.; Kohn, A.; Harding, M. E.; Diezemann, G.; Hinze, G.; Basche, T.; Gauss, J. *J. Chem. Phys.* **2008**, *128*, 074505.

(20) Howard, I. A.; Laquai, F.; Keivanidis, P. E.; Friend, R. H.; Greenham, N. C. *J. Phys. Chem. C* **2009**, *113*, 21225.

(21) Schlosser, M.; Lochbrunner, S. *J. Phys. Chem. B* **2006**, *110*, 6001.

(22) Schubert, A.; Settels, V.; Liu, W. L.; Würthner, F.; Meier, C.; Fink, R. F.; Schindlbeck, S.; Lochbrunner, S.; Engels, B.; Engel, V. *J. Phys. Chem. Lett.* **2013**, *4*, 792.

(23) Scholes, G. D.; Rumbles, G. *Nat. Mater.* **2006**, *5*, 683.

(24) Spano, F. C.; Meskers, S. C. J.; Hennebicq, E.; Beljonne, D. *J. Am. Chem. Soc.* **2007**, *129*, 7044.

(25) Scholz, R.; Kobitski, A. Y.; Zahn, D. R. T.; Schreiber, M. *Phys. Rev. B* **2005**, *72*, 245208.

(26) Seibt, J.; Eisfeld, A. *J. Chem. Phys.* **2012**, *136*, 024109.

(27) Kamm, V.; Battagliarin, G.; Howard, I. A.; Pisula, W.; Mavrinskiy, A.; Li, C.; Müllen, K.; Laquai, F. *Adv. Energy Mater.* **2011**, *1*, 297.

(28) Erwin, P.; Thompson, M. E. *Appl. Phys. Lett.* **2011**, *98*, 223305.

(29) Lunt, R. R.; Benziger, J. B.; Forrest, S. R. *Adv. Mater.* **2010**, *22*, 1233.

(30) Kurrle, D.; Pflaum, J. *Appl. Phys. Lett.* **2008**, *92*, 133306.

(31) Stehr, V.; Fink, R. F.; Engels, B.; Pflaum, J.; Deibel, C. *J. Chem. Theory Comput.* **2014**, *10*, 1242.

(32) Stehr, V.; Engels, B.; Deibel, C.; Fink, R. F. *J. Chem. Phys.* **2014**, *140*, 024503.

(33) Heinemeyer, U.; Scholz, R.; Gisslén, L.; Alonso, M. I.; Ossó, J. O.; Garriga, M.; Hinderhofer, A.; Kytka, M.; Kowarik, S.; Gerlach, A.; Schreiber, F. *Phys. Rev. B* **2008**, *78*, 085210.

(34) Scholz, R.; Schreiber, M. *Chem. Phys.* **2006**, *325*, 9.

(35) Schwoerer, M.; Wolf, C. H. *Organic Molecular Solids*; Wiley-VCH Verlag GmbH & Co. KGaA: Weinheim, 2007.

(36) May, V.; Kühn, O. *Charge and Energy Transfer Dynamics in Molecular Systems*; Wiley-VCH: Weinheim, 2004.

(37) Spano, F. C. *Acc. Chem. Res.* **2010**, *43*, 429.

(38) Spano, F. C. *Annu. Rev. Phys. Chem.* **2006**, *57*, 217.

(39) Bredas, J. L.; Beljonne, D.; Coropceanu, V.; Cornil, J. *Chem. Rev.* **2004**, *104*, 4971.

(40) Martinelli, N. G.; Olivier, Y.; Athanasopoulos, S.; Ruiz Delgado, M. C.; Pigg, K. R.; da Silva Filho, D. A.; Sánchez-Carrera, R. S.; Venuti, E.; Della Valle, R. G.; Brédas, J. L.; Beljonne, D.; Cornil, J. *ChemPhysChem* **2009**, *10*, 2265.

(41) Coropceanu, V.; Cornil, J.; da Silva, D. A.; Olivier, Y.; Silbey, R.; Bredas, J. L. *Chem. Rev.* **2007**, *107*, 926.

(42) Ortmann, F.; Bechstedt, F.; Hannewald, K. *New J. Phys.* **2010**, *12*, 023011.

(43) Hannewald, K.; Stojanovi, V. M.; Schellekens, J. M. T.; Bobbert, P. A. *Phys. Rev. B* **2004**, *69*, 075211.

(44) Nan, G.; Yang, X.; Wang, L.; Shuai, Z.; Zhao, Y. *Phys. Rev. B* **2009**, *79*, 115203.

(45) Yamagata, H.; Norton, J.; Hontz, E.; Olivier, Y.; Beljonne, D.; Brédas, J. L.; Silbey, R. J.; Spano, F. C. *J. Chem. Phys.* **2011**, *134*, 204703.

(46) Gangilenka, V. R.; Titova, L. V.; Smith, L. M.; Wagner, H. P.; DeSilva, L. A. A.; Gisslén, L.; Scholz, R. *Phys. Rev. B* **2010**, *81*, 155208.

(47) Grimme, S. *J. Chem. Phys.* **2003**, *118*, 9095.

(48) Hellweg, A.; Grün, S. A.; Hättig, C. *Phys. Chem. Chem. Phys.* **2008**, *10*, 4119.

(49) Bundgen, P.; Engels, B.; Peyerimhoff, S. D. *Chem. Phys. Lett.* **1991**, *176*, 407.

(50) Engels, B. *J. Chem. Phys.* **1994**, *100*, 1380.

(51) Stanton, J. F.; Bartlett, R. J. *J. Chem. Phys.* **1993**, *98*, 7029.

(52) Hättig, C.; Köhn, A. *J. Chem. Phys.* **2002**, *117*, 6939.

(53) Zhao, H. M.; Pfister, J.; Settels, V.; Renz, M.; Kaupp, M.; Dehm, V. C.; Würthner, F.; Fink, R. F.; Engels, B. *J. Am. Chem. Soc.* **2009**, *131*, 15660.

(54) Grimme, S. *J. Comput. Chem.* **2004**, *25*, 1463.

(55) Grimme, S. *J. Comput. Chem.* **2006**, *27*, 1787.

(56) Becke, A. D. *Phys. Rev. A* **1988**, *38*, 3098.

(57) Lee, C. T.; Yang, W. T.; Parr, R. G. *Phys. Rev. B* **1988**, *37*, 785.

(58) Schäfer, A.; Huber, C.; Ahlrichs, R. *J. Chem. Phys.* **1994**, *100*, 5829.

(59) Weigend, F.; Haser, M.; Patzelt, H.; Ahlrichs, R. *Chem. Phys. Lett.* **1998**, *294*, 143.

(60) Weigend, F.; Haser, M. *Theor. Chem. Acc.* **1997**, *97*, 331.

(61) Schäfer, A.; Horn, H.; Ahlrichs, R. *J. Chem. Phys.* **1992**, *97*, 2571.

(62) Eichkorn, K.; Treutler, O.; Ohm, H.; Haser, M.; Ahlrichs, R. *Chem. Phys. Lett.* **1995**, *242*, 652.

(63) Eichkorn, K.; Weigend, F.; Treutler, O.; Ahlrichs, R. *Theor. Chem. Acc.* **1997**, *97*, 119.

(64) Liu, W. Ph.D. thesis, Institute of Physical and Theoretical Chemistry, University of Würzburg, Würzburg, Germany, 2011.

(65) *TURBOMOLE V6.1 2009*; University of Karlsruhe and Forschungszentrum Karlsruhe GmbH: Karlsruhe, Germany, 2007.

(66) So, F. F.; Forrest, S. R. *Phys. Rev. Lett.* **1991**, *66*, 2649.

(67) Spano, F. C.; Yamagata, H. *J. Phys. Chem. B* **2011**, *115*, 5133.

(68) Gierschner, J.; Huang, Y. S.; Van Averbeke, B.; Cornil, J.; Friend, R. H.; Beljonne, D. *J. Chem. Phys.* **2009**, *130*, 044105.

(69) Havil, J.; Dyson, F. *Gamma: Exploring Euler's Constant*; Princeton University Press: Princeton, 2003.

(70) Ponder, J. W.; Wu, C. J.; Ren, P. Y.; Pande, V. S.; Chodera, J. D.; Schnieders, M. J.; Haque, I.; Mobley, D. L.; Lambrecht, D. S.; DiStasio, R. A., Jr.; Head-Gordon, M.; Clark, G. N. I.; Johnson, M. E.; Head-Gordon, T. *J. Phys. Chem. B* **2010**, *114*, 2549.

(71) Ponder, J. W. *TINKER 5.09*; Washington University School of Medicine, St. Louis, MO, 2010, http://dasher.wustl.edu/tinker/.

(72) Stone, A. J. *J. Chem. Theory Comput.* **2005**, *1*, 1128.

(73) Stone, A. J. *GDMA 2.2*; Emmanuel College: Cambridge, U.K., 2011, http://www-stone.ch.cam.ac.uk/programs.html.

(74) Frisch, M. J.; Trucks, G. W.; Schlegel, H. B.; Scuseria, G. E.; Robb, M. A.; Cheeseman, J. R.; Montgomery, J. A., Jr.; Vreven, T.; Kudin, K. N.; Burant, J. C.; Millam, J. M.; Iyengar, S. S.; Tomasi, J.; Barone, V.; Mennucci, B.; Cossi, M.; Scalmani, G.; Rega, N.; Petersson, G. A.; Nakatsuji, H.; Hada, M.; Ehara, M.; Toyota, K.; Fukuda, R.; Hasegawa, J.; Ishida, M.; Nakajima, T.; Honda, Y.; Kitao, O.; Nakai, H.; Klene, M.; Li, X.; Knox, J. E.; Hratchian, H. P.; Cross, J. B.; Bakken, V.; Adamo, C.; Jaramillo, J.; Gomperts, R.; Stratmann, R. E.; Yazyev, O.; Austin, A. J.; Cammi, R.; Pomelli, C.; Ochterski, J. W.; Ayala, P. Y.; Morokuma, K.; Voth, G. A.; Salvador, P.; Dannenberg, J. J.; Zakrzewski, V. G.; Dapprich, S.; Daniels, A. D.; Strain, M. C.; Farkas, O.; Malick, D. K.; Rabuck, A. D.; Raghavachari, K.; Foresman, J. B.; Ortiz, J. V.; Cui, Q.; Baboul, A. G.; Clifford, S.; Cioslowski, J.; Stefanov, B. B.; Liu, G.; Liashenko, A.; Piskorz, P.; Komaromi, I.; Martin, R. L.; Fox, D. J.; Keith, T.; Al-Laham, M. A.; Peng, C. Y.; Nanayakkara, A.; Challacombe, M.; Gill, P. M. W.; Johnson, B.; Chen, W.; Wong, M. W.; Gonzalez, C.; Pople, J. A. *Gaussian 03*; Gaussian Inc.: Wallingford, CT, 2003.

(75) Tafipolsky, M.; Schmid, R. *J. Phys. Chem. B* **2009**, *113*, 1341.

(76) Tafipolsky, M.; Engels, B. *J. Chem. Theory Comput.* **2011**, *7*, 1791.

(77) Spackman, M. A. *Chem. Phys. Lett.* **2006**, *418*, 158.

(78) Ansorg, K.; Tafipolsky, M.; Engels, B. *J. Phys. Chem. B* **2013**, *117*, 10093.

(79) Bellinger, D. Diploma thesis. University of Würzburg, Würzburg, Germany, 2012.

(80) Podolsky, B. *Phys. Rev.* **1928**, *32*, 812.

(81) Nauts, A.; Chapuisat, X. *Mol. Phys.* **1985**, *55*, 1287.

(82) Feit, M. D.; Fleck, J. A. *J. Comput. Phys.* **1982**, *47*, 412.

(83) Kosloff, R.; Tal-Ezer, H. *Chem. Phys. Lett.* **1986**, *127*, 223.

(84) *Conical Intersections: Electronic Structure, Dynamics and Spectroscopy*; Domcke, W., Yarkony, D. R.; Köppel, H., Eds.; World Scientific Publishing: Singapore, 2004.

(85) Ziessel, R.; Harriman, A. *Chem. Commun.* **2011**, *47*, 611.

(86) Bulovic, V.; Burrows, P. E.; Forrest, S. R.; Cronin, J. A.; Thompson, M. E. *Chem. Phys.* **1996**, *210*, 1.

(87) Alonso, M. I.; Garriga, M.; Karl, N.; Osso, J. O.; Schreiber, F. *Org. Electron.* **2002**, *3*, 23.

(88) Engel, E.; Koschorreck, M.; Leo, K.; Hoffmann, M. *Phys. Rev. Lett.* **2005**, *95*, 157403.

(89) Shank, C. V.; Ippen, E. P.; Teschke, O. *Chem.Phys.Lett.* **1977**, *45*, 291−294.

(90) Tapping, P. C.; Kee, T. W. *J. Phys.Chem. Lett.* **2014**, *5*, 1040−1047.

(91) Athanasopoulos, S.; Hennebicq, E.; Beljonne, D.; Walker, A. B. *J. Phys. Chem. C* **2008**, *112*, 11532.

(92) Topczak, A. K.; Roller, T.; Engels, B.; Brütting, W.; Pflaum, J. arXiv:1207.1036v1 [cond-mat.mrtl-sci].

(93) Engels, B.; Liu, W.; Pfister, J.; Settels, V.; Zhao, H.; Fink, R. F. Electronic Structure of Organic Materials Investigated by Quantum Chemical Calculations. In *Comprehensive Nanoscience and Technology (NNTC)*; Andrews, D.L., Scholes, G. D., Wiederrecht, G. P., Eds.; Elsevier: Amsterdam, The Netherlands, 2011; Vol *1*, pp 1−22.